International Journal of Heat and Mass Transfer 214 (2023) 124446

Contents lists available at ScienceDirect

International Journal of Heat and Mass Transfer

journal homepage: www.elsevier.com/locate/ijhmt

Investigation of flow behavior in a refrigerator machine room using magnetic resonance velocimetry

Hangfei Dong[a], Chaehyuk Im[a], Chiho Kang[b], Jee-Hyun Cho[c], Ilhoon Jang[a,*], Simon Song[a,*]

[a] Department of mechanical convergence engineering, Hanyang university, Seoul 04763, Korea
[b] Vibration noise project, H&A R&D center, LG electronics, Seoul 08592, Korea
[c] Bio-Chemical Analysis Team, Korea Basic Science Institute, Cheongju 28119, Korea

ARTICLE INFO

Article history:
Received 25 March 2023
Revised 17 May 2023
Accepted 22 June 2023
Available online 3 July 2023

Keywords:
Magnetic resonance velocimetry (MRV)
Refrigerator machine room
Turbulent kinetic energy (TKE)
Flow uniformity

ABSTRACT

This study aims to improve the energy efficiency and reduce flow noise in a refrigerator machine room by investigating the flow behavior using magnetic resonance velocimetry (MRV). A 1/2 scale model of the machine room was fabricated using stereolithography 3D printing, and the 3-dimensional mean velocity and turbulent kinetic energy (TKE) field were measured. Results from the reference model showed highly non-uniform flow distribution and high TKE regions. An improved machine room geometry was proposed, which led to an increase in mean flowrate through the condenser by 17.3% and a reduction in high TKE regions by over 77%, potentially resulting in improved energy efficiency and reduced turbulence-induced noise. These findings demonstrate the effectiveness of MRV in analyzing the flow behavior of complex 3D geometry such as the refrigerator machine rooms. The proposed improvements, including repositioning of flow-blocking pillars, relocating refrigerant pipes, changing inlet configurations, and increasing the area of inlet and outlet grilles, were validated using MRV. The results also confirm the accuracy of the MRV measurements, which were validated using an electromagnetic flowmeter. These findings have implications for the practical application of cooling systems and highlight the potential of MRV for future research in analyzing fan noise and applying MRV to models with built-in fans.

1. Introduction

In recent years, the market demand for home appliances with high energy efficiency and low noise, particularly premium products, has increased significantly, prompting extensive research in this area [1–4]. Heat and noise in home appliances are typically generated by specific components within the system. For refrigerators, the compressor and condenser are the primary sources of heat and noise [5]. Given the importance of both components in the operation of the refrigerator system, it is crucial to enhance the performance of the compressor and condenser to develop high-energy efficient and low-noise refrigerators.

The compressor and condenser are typically located at the bottom rear section of a refrigerator, known as the machine room. The room is designed with a ventilation system to dissipate the heat produced inside. However, when the flow environment inside the machine room is not properly considered, the proportion of air passing through the condenser is significantly reduced, and a large amount of flow-induced noise is generated due to turbulence. This is because a turbulent flow generates vortices that create pressure fluctuations and sound waves, resulting in flow-induced noise [6,7]. Therefore, it is crucial to ensure a uniform flow distribution around the condenser and improve the machine room structure to effectively discharge internal heat to the outside, thereby maximizing heat exchange performance and minimizing noise.

To improve the internal structure of the machine room, measuring internal flow is essential. In the past, hot wire anemometer [8] or pitot tube techniques were utilized in the refrigerator to measure air flow speed. However, these point-wise (1D) techniques had limitations in analyzing accurate spatial flow distribution due to their invasive nature. Subsequently, particle image velocimetry (PIV) was frequently used to measure 2D flow distribution of the upstream and downstream of the evaporator for two refrigerator models [9] to confirm factors causing flow non-uniformity. Kim et al. [10] used computational fluid dynamics (CFD) to analyze flow around the grille in the machine room and improved the grille's shape to increase flow rate through the condenser. However, PIV cannot visualize flow in an opaque and complex environment, such as the machine room's interior. Moreover, it is difficult or requires

* Corresponding author.
E-mail addresses: iroonjang@hanyang.ac.kr (I. Jang), simonsong@hanyang.ac.kr (S. Song).

https://doi.org/10.1016/j.ijheatmasstransfer.2023.124446

bulky, complex equipment to measure the entire 3D flow field. Additionally, CFD research using simple 2D models or simplified structures for analyzing flow in the refrigerator machine room has limitations in accurately understanding the actual flow characteristics.

Magnetic resonance velocimetry (MRV) is a non-invasive technique that employs magnetic resonance imaging (MRI) to visualize fluid flow. MRV is particularly useful in studying opaque and complex flows, as it can measure three-dimensional velocity, temperature, density, and TKE fields [11–14]. Therefore, there has been a recent surge in the use of MRV in complex flow measurement research. For instance, Lee et al. [15]. utilized MRV and omni-directional integration (ODI) technique to visualize mean flow velocity and calculate the pressure field inside a vacuum cleaner nozzle. Similarly, Davidson et al. [16]. and Baek et al. [17]. employed MRV to study the complex internal cooling flows within gas turbine blades. Schmidt et al. [18]. validated MRV's ability to accurately measure turbulence in complex flow patterns at high Reynolds numbers. Therefore, using MRV to measure fluid flow inside a refrigerator machine room would enable a precise understanding of the flow characteristics, which can help improve internal flow, thereby increasing energy efficiency and reducing refrigerator noise.

The objective of this study is to investigate the feasibility of measuring 3D mean velocity and TKE inside the refrigerator machine room using magnetic resonance velocimetry (MRV) and enhancing the internal flow of a commercially available LG Electronics refrigerator (M349SE model). To achieve this goal, we construct an experimental model of the refrigerator machine room and internal components using 3D printing. Based on the measured results, we identify the internal geometry that causes non-uniform flow in the machine room and propose an improved internal geometry. It is important to note that the change in internal geometry is limited to factors that can be incorporated into the actual machine room design. Finally, we compare the velocity and TKE in the improved machine room to confirm the improvement of the internal flow. Our findings demonstrate the potential of MRV in improving the energy efficiency and noise reduction of refrigerators by enhancing the internal flow through modifications to the internal geometry.

2. Experimental methods

Fig. 1 shows a three-dimensional CAD image of the refrigerator machine room model. The machine room contains a condenser, compressor, refrigerant pipes, fan, 4 inlets, and 5 outlets. The inlets and outlets are positioned on the right and left sides of the fan, respectively (Fig. 1a). Under the rated output condition (medium speed), the fan rotates at 730 rpm and generates flow within the machine room. Prior to the MRV experiments, we confirmed that the airflow rate through outlet 2, with the other outlets (outlets 1, 3, 4, and 5) closed, was 397.6 liters per minute (LPM) under the above condition. However, for the MRV experiments, we used an external pump to drive flow through the machine room and a stationary fan system that only allows non-metallic materials inside. Additional details on how we measured the airflow rate are provided in supplementary material1.

The machine room model was installed at the rear of the test section, as illustrated in Fig. 1d and shown in the inset optical picture of Fig. 2. To prevent unnecessary flow mixing of the inlet and outlet flows, a partition dividing the flow entrance from the exit was positioned in the middle. Thus, the fluid entering the test section passed through the machine room model and was discharged through the outlets. Upstream of the test section, a flow conditioner was installed to reduce swirls and vortices and provide more uniform flow at the entrance. Since metals are not allowed in the MRI scan room area to prevent magnetic field distortion, all experimental components of the test section were made of plastic materials. The outer case and connecting parts were made of machine-processed polycarbonate, while all other parts were produced through stereolithography (SLA) 3D printing (Form 3 L, formlabs, USA). The resolution of the 3D printing was 50 μm, and clear photopolymer resin was used as the printing material. All 3D printed parts were printed separately and then assembled. We fabricated two MRV models, the reference model and the improved model, and both models had the same structure and size, except for the elements that were improved.

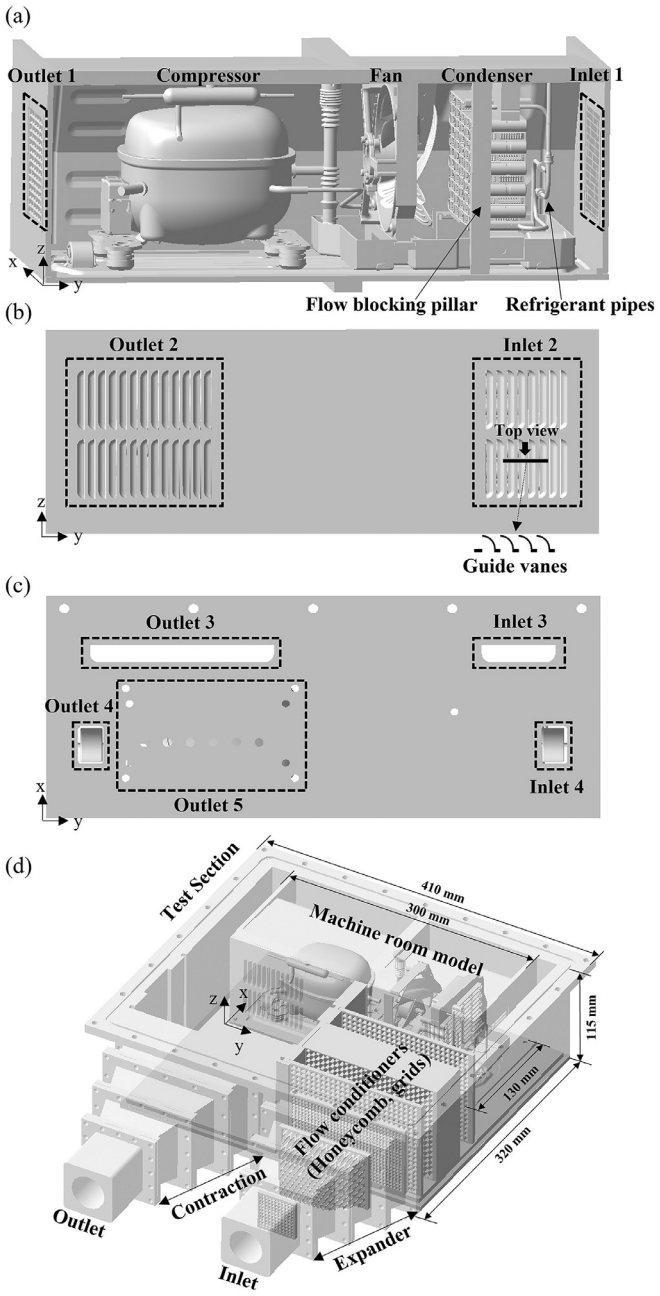

Fig. 1. 3D model of the refrigerator machine room for MRV. (a) The machine room is viewed from the back of the refrigerator without the rear panel. Components such as compressor, fan, and condenser are placed inside the room, and inlet 1 and outlet 1 are at each side. The top and refrigerator front sides are blocked and (b) the rear panel and (c) the bottom panel have inlets and outlets. (d) A schematic of the entire test section with expander, flow conditioners, machine room model and contraction.

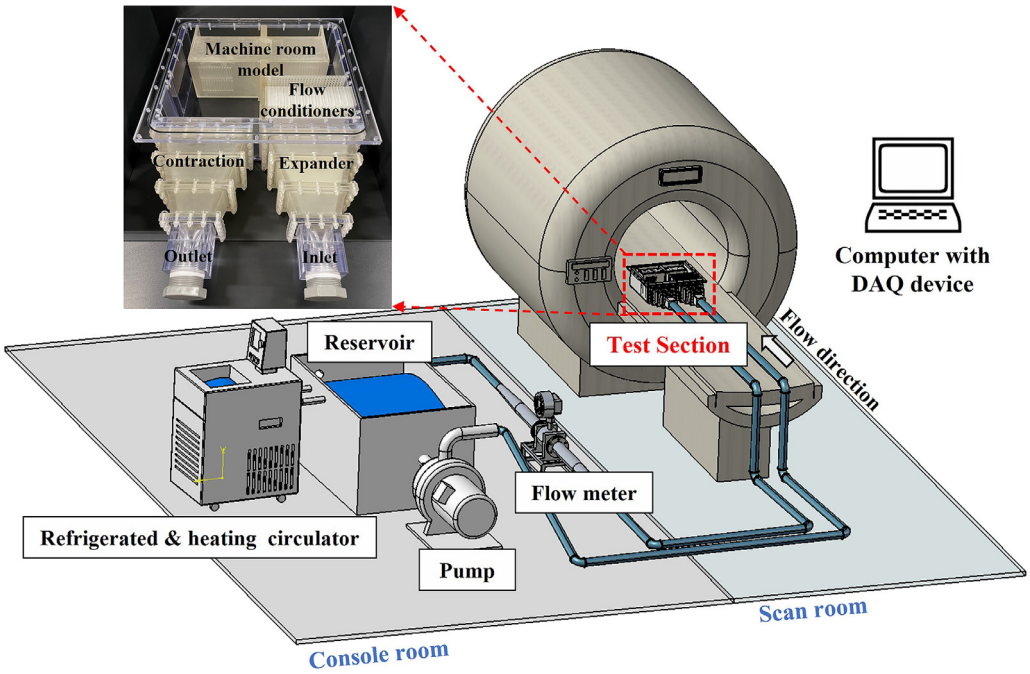

Fig. 2. A schematic of the closed-loop flow circuit for the MRV experiment. The test section placed in a bed of the scanner is connected to the flow meter, reservoir, and pump in the console room through pipe systems. The flow entered the test section passes through the flow conditioner and machine room model sequentially and exits. Control of experiments and data acquisitions are conducted via a computer with a DAQ device.

Table 1
Comparison of flow conditions in the MRV experiment. Reynolds similarity between the actual model and MRV model was used to determine the flow conditions.

Model	Scale	Hydraulic diameter [cm]	Fluid	Kinematic viscosity [m^2/s]	*Re*	Q_{out} [LPM]	Mean velocity [cm/s]
Actual	1	1.670	Air	1.506E-5 (20 °C)	760	397.6	68.5
MRV	0.5	0.835	Water	1.0023E-6 (20 °C)	760	13.2	9.1

As MRV measurement uses water as the working fluid, it is necessary to perform Reynolds similarity to reflect the flow characteristics of air in the actual model. The Reynolds number is calculated based on the hydraulic diameter () and mean velocity (V) at outlet 2 (Fig. 1b), and the dynamic viscosity (ν) of the working fluid at a specific temperature (20 °C) in the machine room model, using the following formula:

$$Re = \frac{VD_h}{\nu}. \quad (1)$$

The calculated Reynolds number was 760. However, since the machine room model for MRV was fabricated at 1/2 the actual size to fit inside an MRI torso coil, the hydraulic diameter was reduced. Therefore, we calculated the flow rate for the MRV experiment by considering the changes in the working fluid and size of the model. Detailed flow conditions for the Reynolds similarity are summarized in Table 1.

Fig. 2 shows the flow circuit used for MRV measurement in a closed-loop system. The MRV experiments were conducted using a 3T human MRI system (Achieva 3T, Philips, Netherlands) located at the Ochang campus of the Korea Basic Science Institute (KBSI, Chungju, Korea). The assembled test section was wrapped using a 16-channel torso coil designed for a human body and placed inside the MR scanner. The flow supply system, located in the console room adjacent to the scan room, comprised a three-phase pump (PA-1000SS-T, Hanil Electrics, Korea), inverter (SV015 IG5A-1, LSIS, Korea), electromagnetic flowmeter (KTM-800, Korea Flowmeter, Korea), reservoir, and piping components. The temperature of the working fluid was maintained at 20 °C during the experiment using a refrigerated and heating circulator (RW3–1025, Jeio Tech, Korea). To achieve a high signal-to-noise ratio (SNR) in MRV measurement, a 20 mM aqueous solution of $CuSO_4$ was used as the working fluid [19], which has almost the same viscosity and flow characteristics as water.

The mean velocity measurement was performed using the Qflow ("Quantitative flow measurement") sequence program built into the Philips MRI scanner, which employs a six-point phase contrast method [20] for velocity encoding. The measurement was conducted using a field of view (FOV) of 360 × 176 × 130 mm, with 0.5 mm isotropic voxels. The repetition and echo times were set to a minimum of 5.5 ms and 3.0 ms, respectively, and a flip angle of 15° was used. To prevent aliasing and minimize uncertainty, a velocity encoding (VENC) of 20 cm/s was applied. To correct background noise caused by magnetic field inhomogeneity, the same MRI parameters were used for both the flow-on and flow-off conditions, and the resulting data were subtracted [19,21,22]. To improve the reliability of the measured data and reduce uncertainty, the number of signal averages (NSA) was set to 4, and the average of two sets of flow-on and flow-off data was used [23,24]. The measurement uncertainty of the mean velocity for each velocity component in two sets of flow-on data with identical MRI scan parameters and flow conditions within the region of interest (ROI) of all flow regions was calculated using the equation proposed by Bruschewski et al. [25], given by:

$$\sigma_u = \frac{1}{\sqrt{2NSA}}\sqrt{Var\{u_1(ROI) - u_2(ROI)\}}, \quad (2)$$

where NSA is the number of signal averages, factor 2 arises from the subtraction of two sets of data, and u indicates the same velocity component in each data set.

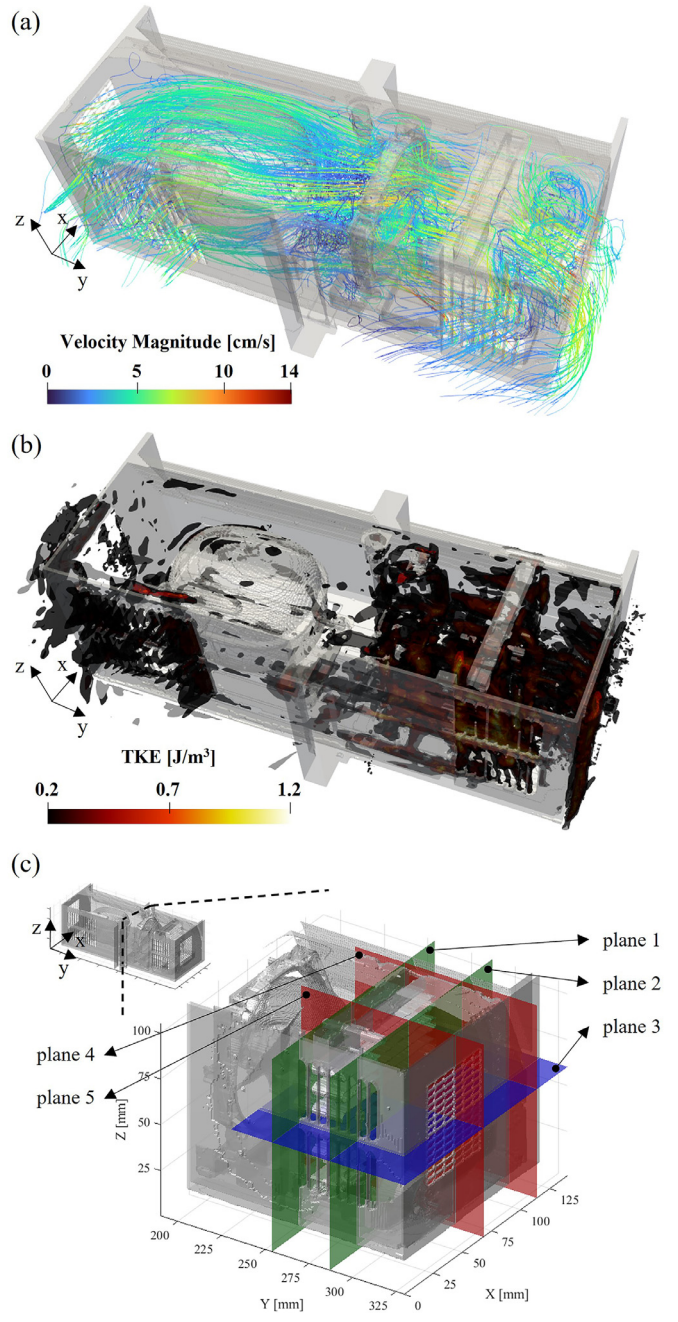

Fig. 3. Overall flow characteristics and five critical planes around the condenser. (a) Streamlines showing the flows inside and outside of the machine room. The color indicates the velocity magnitude. (b) Turbulent kinetic energy field of the reference model visualized by the isosurface of TKE ranging from 0.2 to 1.2 J/m^3. (c) The enlarged 3D geometry with five different planes for the reference model. Planes 1 and 2 are the xz-plane, plane 3 is the xy-plane, and planes 4 and 5 are the yz-plane. Each plane is located at $y = 255$ mm, $y = 280$ mm, $z = 60$ mm, $x = 118$ mm, and $x = 67$ mm, respectively.

Besides the mean velocity, turbulence kinetic energy was also measured using Dyverfeldt's theory [26,27], which involves estimating the turbulence intensity through the signal magnitude ratio between the reference scan, S(0), without applying the bipolar gradient pulse and the scan, S(k_v), with the bipolar gradient pulse. The turbulence intensity in one direction, $\bar{u}'_i$, is calculated using the following equation:

$$\bar{u}'_i = \sqrt{\frac{2\ln\left(\frac{S(0)}{S(k_v)}\right)}{k_v^2}} \tag{3}$$

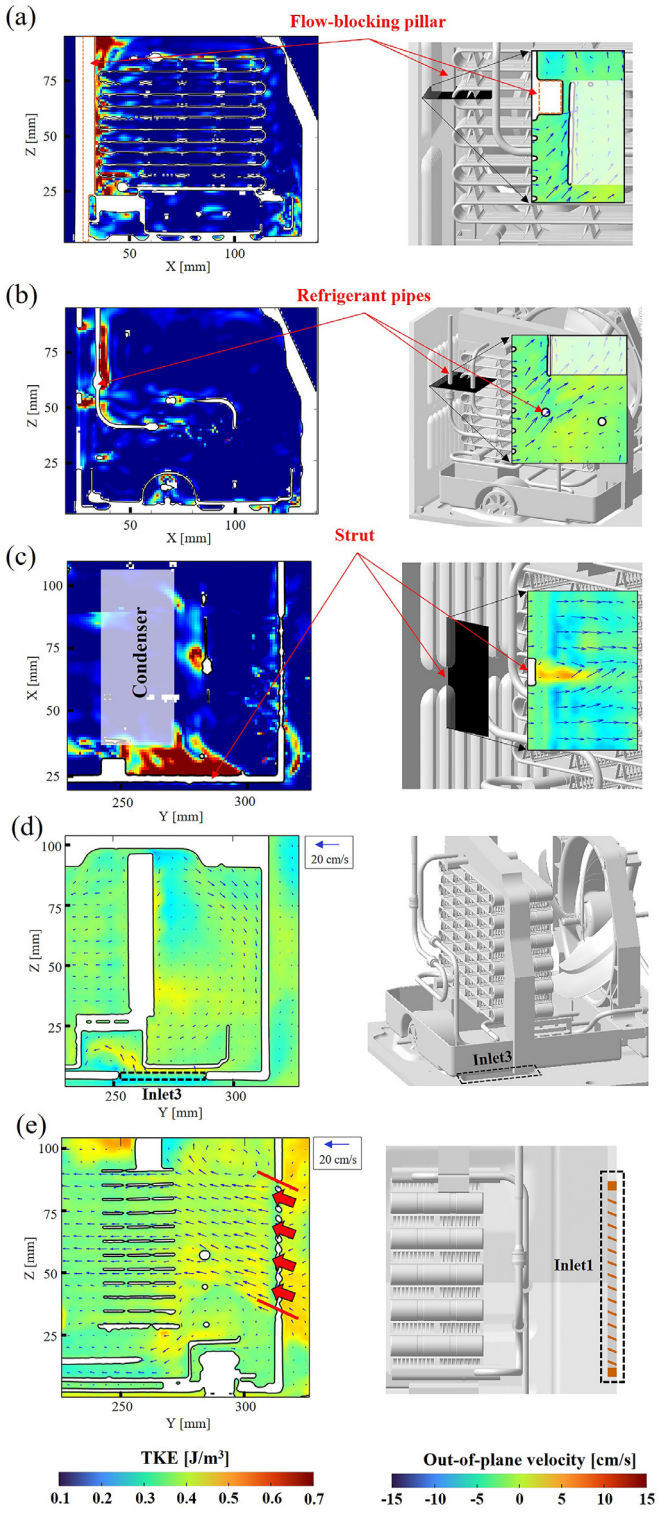

Fig. 4. Detailed flow characteristics at the five representative planes of the reference model. TKE contour on (a) plane 1 in the xz-plane at $y = 255$ mm, (b) plane 2 in the xz-plane at $y = 280$ mm, and (c) plane 3 in the xy-plane at $z = 60$ mm. Each contains the neighborhood geometry and the essential flow features. Velocity vector contour on (d) plane 4 in the yz-plane at $x = 118$ mm, and (e) plane 5 in the yz-plane at $x = 67$ mm.

Table 2
MRI scan parameters.

	Mean velocity	TKE
Scan mode	3D	3D
Slice orientation	Coronal	Coronal
FOV [mm]	360 × 176× 130	360 × 176× 130
Voxel size [mm]	0.5× 0.5× 0.5	1.0 × 1.0 × 1.0
TR, TE [ms]	5.5, 3.0	7.1, 3.4
VENC [cm/s]	20	7
Flip angle	15	15
NSA	4	15
Flow compensation	on	off
Pump condition	off/on/on/off	on/on
Total scan duration [hour]	3	4

Table 3
Flow conditions.

		Target value	Reference model (relative error)	Improved model (relative error)
Temperature [°C] – Thermocouple		20.0	20.1 (0.5%)	20.2 (1.0%)
Flowrate [LPM]	Flowmeter	13.2	13.2 (<0.8%)	13.3 (0.8%)
	MRV (Inlet total)		13.2 (<0.8%)	13.4 (1.5%)
	MRV (Outlet total)		13.4 (1.5%)	13.5 (2.3%)

where k_v is the flow sensitivity calculated by π/VENC. The value of VENC affects the sensitivity of turbulence intensity, with the best sensitivity attained at $\overline{u_i'} = \text{VENC} / \pi$, corresponding to a signal magnitude ratio S(k_v)/S(0) of $e^{-1/2}$ [26]. For TKE measurement, VENC was set to 7 cm/s. The spatial resolution was 1 mm isotropic, and the repetition and echo times were set to a minimum of 7.1 ms and 3.4 ms, respectively. The NSA was raised to 15, and measurements were taken twice with the flow-on. TKE was then calculated using the equation:

$$\text{TKE} = \frac{1}{2}\,\rho\left(\overline{u_1'u_1'} + \overline{u_2'u_2'} + \overline{u_3'u_3'}\right). \quad (4)$$

where ρ is the fluid density. The detailed MRI parameters for mean velocity and TKE measurements are summarized in Table 2.

The raw data measured by MRV was extracted using the Pack'n Go tool (Gyrotool LLC, Zurich, Switzerland). Due to non-linear effects of the imaging gradients in MRI scanners, distortion increases as the measured point moves away from the center, particularly in large FOVs. To correct for these distortions, the collected data were reconstructed using ReconFrame (Gyrotool LLC, Zurich, Switzerland). The collected data is in the form of a matrix, which includes 3D coordinate values, velocity, and TKE for each voxel. Further analysis such as averaging, setting a threshold, and drawing plots were performed using Matlab (R2022b, Mathworks, USA). Additionally, we utilized Paraview (Kitware, USA) to visualize the analyzed results, such as streamlines and TKE isosurfaces.

3. Results and discussion

3.1. Validation of MRV flow conditions

Table 3 displays the target values of temperature and flowrate required to achieve Reynolds similarity, as well as the estimated values obtained from MRV results for the reference and improved models. To measure the flow conditions at the test section inlet, a K-type thermocouple (Omega Engineering, USA) was installed in the reservoir. Additionally, an electromagnetic flowmeter (KTM-800, Korea Flowmeter, Korea) was placed in the middle of the flow circuit. The average temperature of the working fluid during the scan time was 20±1°C for both the reference and improved models, and remained stable throughout the experiment, ensuring the accuracy and consistency of measurements. The average flowrate measured by the electromagnetic flowmeter was 13.2±0.2 LPM and 13.3±0.2 LPM for the reference and improved models, respectively, which is close to the target flowrate of 13.2 LPM. The accuracy of the MRV measurements was verified by comparing the flowrate obtained from MRV and flowmeter. As presented in Table 3, the total inlet and outlet flowrates of the reference model (13.2±0.7 LPM and 13.4±0.7 LPM, respectively) exhibited negligible discrepancy compared to the flowmeter measurement values. Similarly, for the improved model, the inlet flowrate was 13.4 ± 0.7 LPM, and the outlet flowrate was 13.5 ± 0.7 LPM, indicating that the configured closed-loop flow circuit effectively implemented the target temperature and flowrate and that the MRV experiments were conducted with precision.

Table 4
The measurement uncertainty of mean velocity in the two models.

		σ_u [cm/s]	$\sigma_u/VENC$ [%]
Reference model	V_x	0.25	1.3
	V_y	0.27	1.4
	V_z	0.23	1.2
Improved model	V_x	0.25	1.3
	V_y	0.29	1.5
	V_z	0.21	1.1

Table 5
Fractions of area and flowrate for each inlet and outlet.

	Reference model		Improved model	
	Area	Flowrate	Area	Flowrate
Inlet 1	0.38	0.51	0.65	0.59
Inlet 2	0.50	0.41	0.31	0.40
Inlet 3	0.08	0.06	–	–
Inlet 4	0.04	0.02	0.04	0.01
Total	1.00	1.00	1.00	1.00
Outlet 1	0.29	0.38	0.39	0.48
Outlet 2	0.53	0.53	0.45	0.44
Outlet 3	0.13	0.06	0.12	0.05
Outlet 4	0.02	0.01	0.01	0.01
Outlet 5	0.03	0.02	0.03	0.02
Total	1.00	1.00	1.00	1.00

Table 4 shows the measurement uncertainty of each component of the mean velocity in both models. The V_y component exhibited relatively larger uncertainty values in both models, primarily due to its larger velocity values. Nonetheless, the uncertainties for each velocity component did not show significant changes and remained within 1.5% of the VENC, which is comparable to the results of the MRV challenge [28,29]. Therefore, these uncertainties can be considered negligible.

3.2. Flow characteristics of reference model

To gain insight into the overall flow characteristics, three-dimensional streamlines were plotted in the test section and presented in Fig. 3a. The velocity magnitude ranging from 0 to 14 cm/s was represented by the color of the streamline. The experimental setup involved the flow entering the machine room on the right side, passing through internal components such as the condenser, fan, and compressor, and exiting through the outlets on the left side. MRV technology enabled 3D measurements of the flow around the machine room model, including the bent flow upstream and downstream of the inlets and outlets. The experimental setup was designed to simulate the flow of a refrigerator located in a kitchen, which resulted in narrow passes and bends. The flow rate passing through each inlet and outlet was proportional to its individual area, as presented in Table 5. The streamlines in Fig. 3a represent the characteristics of the main flow of

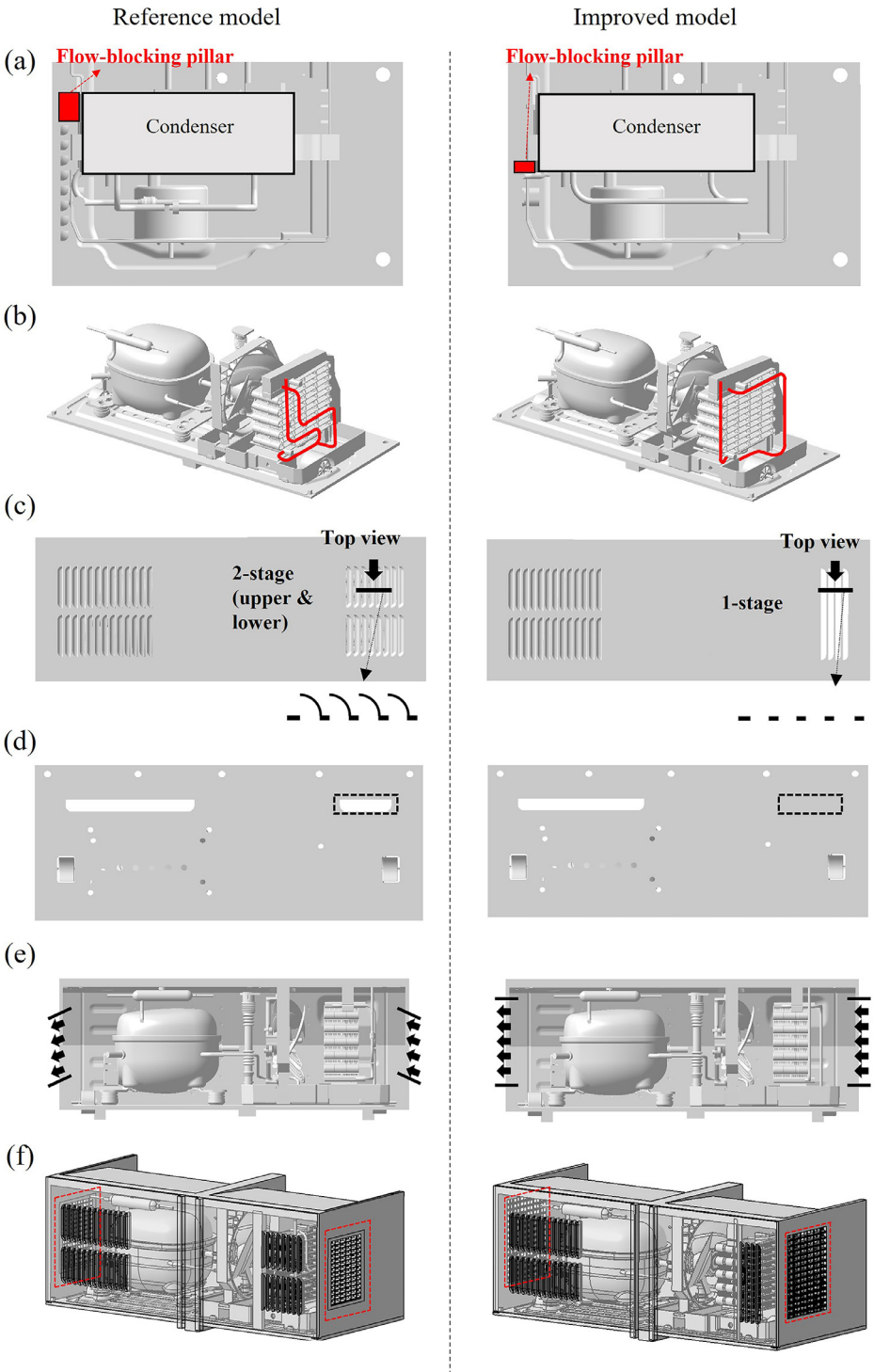

Fig. 5. Comparison of the machine room structures between the reference and improved models. (a) Top view of the flow-blocking pillar displacement, (b) relocation of the refrigerant pipe, (c) three shape changes made to inlet 2, (d) removal of inlet 3 at the bottom panel, (e) change in the grille direction of inlet 1 and outlet 1, and (f) enlargement of the area of inlet 1 and outlet 1. Red dotted boxes are included for convenient size comparison.

the machine room. The guide vanes directing the flow towards the fan caused most of the flow entering inlet 2 on the back panel to bypass or pass the left-hand side of the condenser. Although a stationary fan was used, the wake of the fan resulted in a complex flow field due to the fan blades. The compressor's rounded shape ensured uniform and smooth streamlines around the compressor. Further details will be discussed with Fig. 4. Overall, the MRV experimental setup allowed for a detailed understanding of the flow characteristics around the machine room.

The experimental setup also included independent measurement of TKE in addition to 3D flow velocity. Fig. 3b presents the TKE field of the reference model, visualized by the isosurface of TKE ranging from 0.2 to 1.2 J/m^3. Significant variations in the TKE field were observed in some regions of the machine room. Due to the narrow passage through the condenser and the complex configuration of the machine room inlets, a high TKE was measured around the condenser. The highest TKE levels were found after the guide vane of inlet 2 on the left side of the condenser. In contrast,

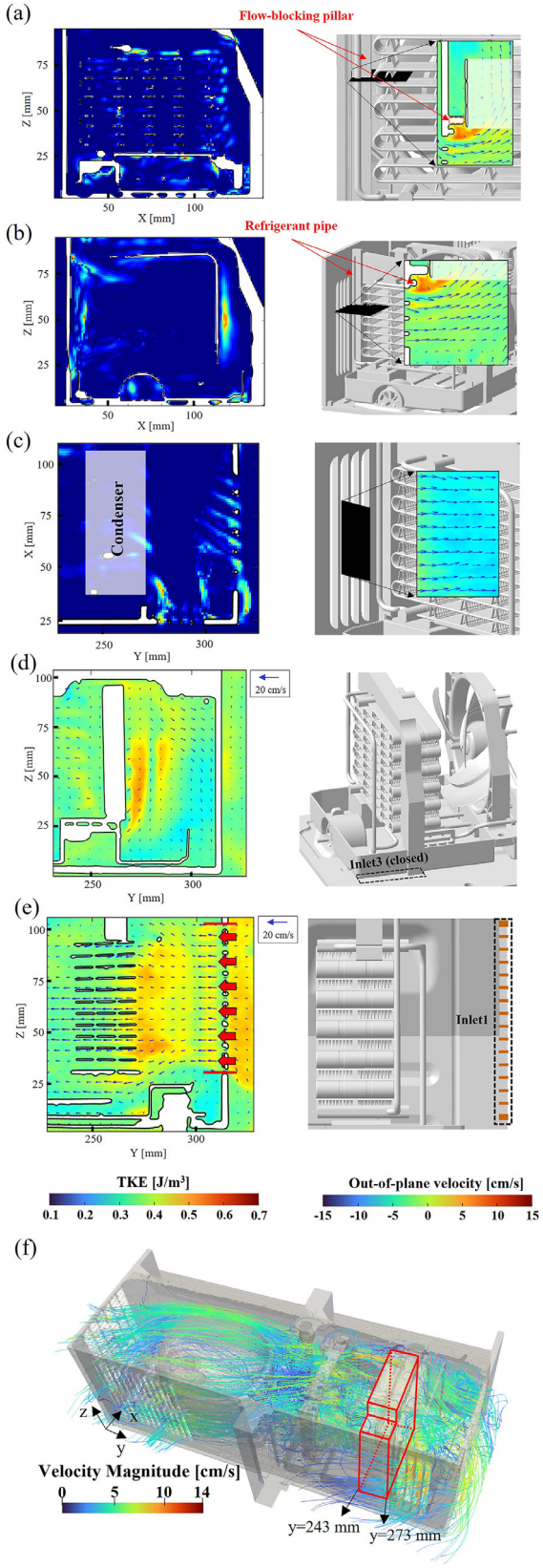

Fig. 6. Detailed flow characteristics at the five representative planes of the improved model. TKE contour on (a) plane 1 in the xz-plane at $y = 255$ mm, (b) plane 2 in the xz-plane at $y = 280$ mm, and (c) plane 3 in the xy-plane at $z = 60$ mm. Each contains the neighborhood geometry and the essential flow features. Velocity vector contour on (d) plane 4 in the yz-plane at $x = 118$ mm, and (e) plane 5 in the yz-plane at $x = 67$ mm. (f) 3D streamline plot showing the flows inside and outside of the machine room. The color represents the velocity magnitude, and red lines indicate the location of the condenser.

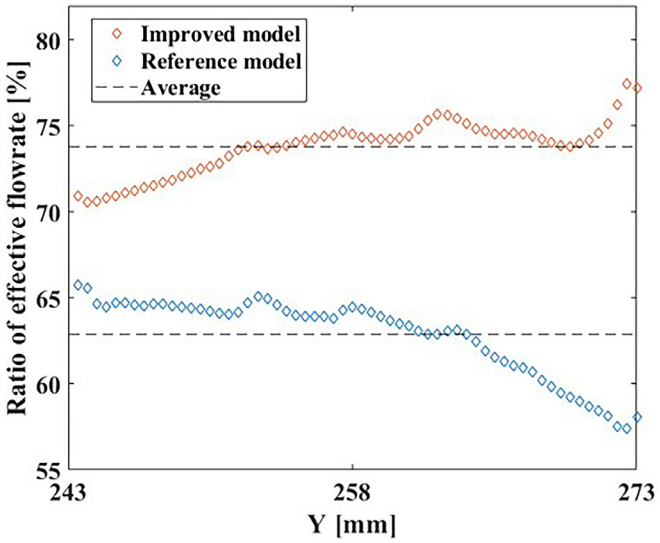

Fig. 7. Ratio of effective flowrate of the reference model to improved model passing through the condenser along the Y-axis.

the surrounding area of the compressor exhibited a TKE level of less than 0.2 J/m^3 due to its large size and smooth shape.

In order to understand the details of flow characteristics inside the reference model, five representative planes were selected in regions where the streamlines were complex and the TKE was high, as depicted in Fig. 3c. The TKE or mean velocity vector contours of the five planes are shown in Fig. 4. First, Fig. 4a shows the TKE contour of the plane 1 across the flow-blocking pillar and condenser. The pillar width is smaller than the condenser width (see the red block of Fig. 5) and there are small gaps between them causing a locally sudden contraction of the flow area. Consequently, these resulted in a local rapid flow and high TKE distribution. Fig. 4b shows the effects of the refrigerant pipe located in front of the condenser (plane 2). The refrigerant pipes partially disrupted the flow entering from inlet 2 on the rear panel and generated a high level of TKEs downstream of the pipes. Fig. 4c (plane 3) indicates the increase in TKE due to the strut located in the center of inlet 2. The strut created a recirculation zone and shear layer downstream, which was found to generate high TKE levels. The velocity vector contour (plane 4) for the flow above inlet 3 located on the bottom of the machine room shows that the flow was blocked and became unnecessarily complicated by the structure located under the condenser as shown in Fig. 4d. Fig. 4e exhibits the central flow field (plane 5) coming from inlet 1. Due to the angle of the grille of inlet 1 facing upwards, the flow towards the condenser was dispersed upwards, causing a secondary flow to occur at the upper zone.

3.3. Structure improvements

Based on the analysis of flow characteristics in the machine room, suggested improvements to the internal structure are presented in Fig. 5. The proposed modifications aim to enhance flow uniformity and increase flow rate through the condenser while reducing TKE, resulting in improved energy efficiency and lower flow-induced noise. The suggested changes are limited to modifications that can be easily applied to the manufacturing process of the machine room. The left column of Fig. 5 shows the reference model, while the right column demonstrates the improved model. Several modifications were proposed, as follows. Firstly, the posi-

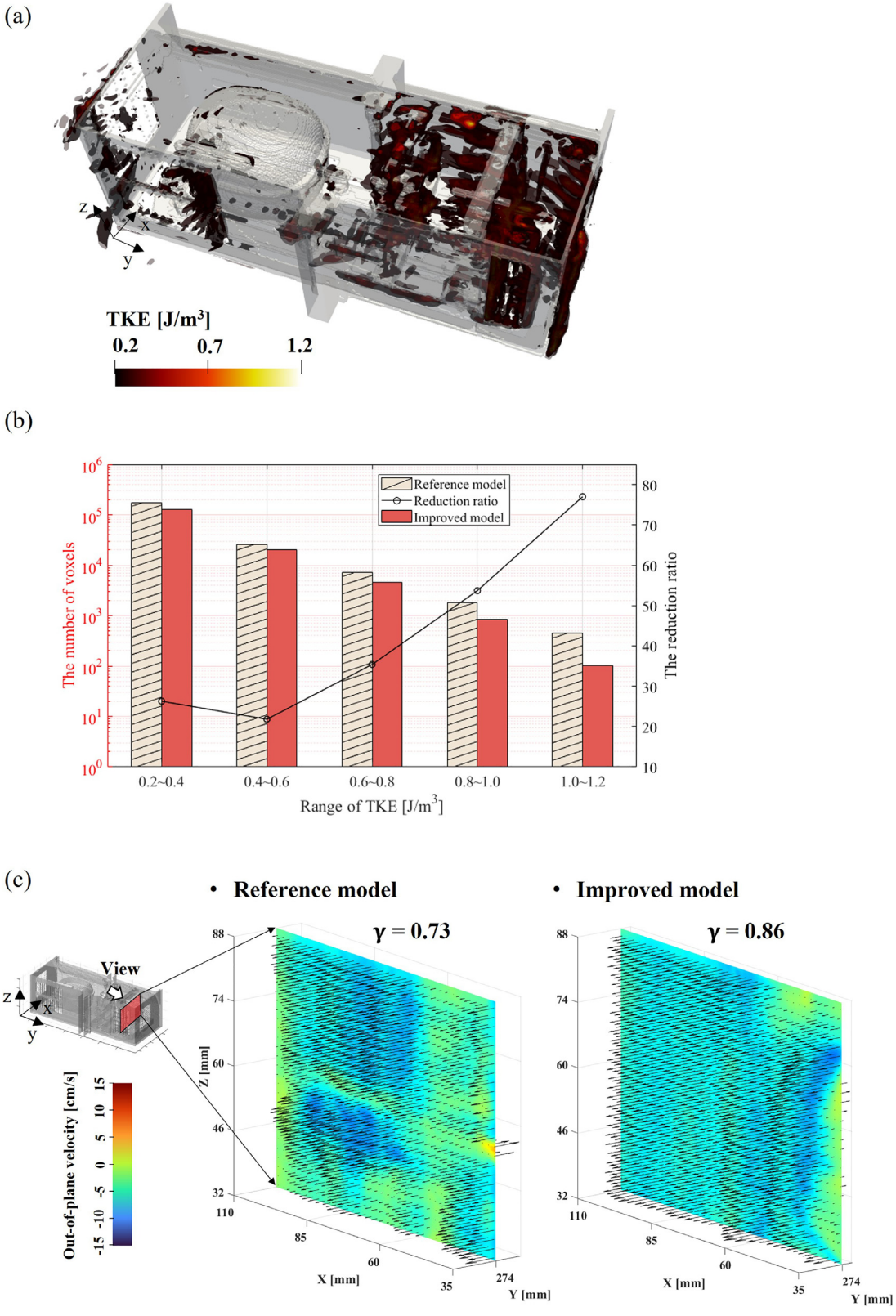

Fig. 8. (a) Turbulent kinetic energy field of the improved model visualized by the isosurface of TKE ranging from 0.2 to 1.2 J/m^3. (b) Comparison of the number of voxels with TKE values ranging from 0.2 to 1.2 J/m^3 between the reference and improved models. The reduction ratio represents the ratio of the number of voxels in the improved model to that of the reference model. (c) 2D flow profile and result of flow uniformity index at the cross-section located before flow entering the condenser.

tion of the flow-blocking pillar (red) was moved slightly upstream to better block the flow from inlet 2 directed towards the left-hand side of the condenser (Fig. 5a). Secondly, the refrigerant pipes were relocated to the edge of the condenser to prevent interference from the inlet flows (Fig. 5b). Thirdly, changes were made to inlet 2 in Fig. 5c, which involved reducing the number of grills (removing the left-hand side grills) to direct more flow towards the condenser front, removing the middle strut by changing the two-stage inlet to one-stage to reduce unnecessary high TKE behind it, and eliminating the guide vanes that previously forced the incoming flow to the left. Furthermore, inlet 3 was closed as shown in Fig. 5d because it had negligible positive effects on the flow characteristics in the machine room. Finally, to make the internal flow more uniform through the condenser, fan, and compressor, the direction of the inlet 1 and outlet 1 grill located on the side panel was changed to a horizontal direction, and the area was increased by 60% each (Fig. 5e and 5f).

3.4. Flow characteristic comparison of reference and improved models

The proposed shape modifications for the improved model were fabricated, and mean velocity and TKE were measured using MRV. Table 5 presents a comparison of flowrate fraction between the reference and improved models. The results showed that the flowrate entering from inlet 1 increased from 51% in the reference model to 59% in the improved model, while the flowrate entering from inlet 2 slightly decreased from 41% to 40% of the total flowrate. These changes were attributed to the increased area of inlet 1, decreased area of inlet 2, and closure of inlet 3. Additionally, the flowrate exiting through outlet 1 increased from 38% to 48%, while the flowrate exiting through outlet 2 decreased from 53% to 44% in the same manner as the inlets.

Fig. 6 provides a detailed analysis of the flow behavior in the improved model, with TKE contour or velocity vector contour plotted for five planes. The results show that the relocation of the flow-blocking pillar (Fig. 5a) had a significant impact on the flow entering from inlet 2, leading to the elimination of a bypass flow and rapid flow bend between the condenser and the rear panel (Fig. 6a). This resulted in a significant decrease in TKE compared to the reference model. The relocation of the refrigerant pipe and the removal of the middle strut in inlet 2 (Fig. 5b and 5c) further reduced the peak TKE values in both cases, as exhibited in Fig. 6b and 6c. The removal of inlet 3 (Fig. 6d) resulted in a more stable flow distribution under the condenser. Additionally, changing the grille angle of inlet 1 to be horizontal and increasing its area by 60% (Fig. 6e) resulted in a uniform horizontal flow entering the condenser and eliminated the secondary flow that occurred in the upper zone. Additionally, the average velocity of the entering flow increases to 3.6 cm/s compared to 2.7 cm/s of the reference model. The overall flow behavior in the improved model is further confirmed by the velocity streamlines plotted in Fig. 6f. It is evident that a significant portion of the flow entered through inlet 2 passes through the condenser.

To compare the performance of the reference and improved models, the throughput ratio of the two model condensers was analyzed. Note that the red line indicates the condenser in Fig. 6f. The ratio of effective flowrate, defined as the ratio of flowrate through the condenser to the total flowrate, was calculated to confirm the performance of the improved model. This was achieved by analyzing the ratio between the downstream plane ($y = 243$ mm) and the upstream plane ($y = 273$ mm) of the condenser. Fig. 7 compares the effective flowrate ratio and shows that the reference model had an average of 63% in the given range. In contrast, the improved model exhibited an average effective flowrate of 74%, which is approximately 17% higher than the reference model. These results indicate that the increased flowrate through the condenser in the improved model is likely to lead to a decrease in the RPM of the fan under the same cooling performance. This, in turn, will result in improved energy efficiency and reduced noise caused by the fan. These implications are important for practical applications of the cooling system, and the results demonstrate the effectiveness of the proposed modifications to the internal structure of the machine room.

Fig. 8a displays the TKE isosurface of a range of 0.2 through 1.2 J/m^3 inside the machine room of the improved model. Compared to the reference model in Fig. 3b, the isosurface in the improved model is significantly reduced, indicating an increase in overall flow uniformity. Fig. 8b provides a quantitative comparison of the number of voxels in each given range of TKE between the two models, as well as the reduction ratio in the number of voxels. The results demonstrate that the number of voxels in the improved model with a TKE range of 0.2 to 0.4 J/m^3 is approximately 26% lower than in the reference model. Additionally, the number of voxels with higher TKE values decreases significantly by 77%, particularly in the TKE range of 1.0 to 1.2 J/m^3. These findings suggest that the proposed modifications to the internal structure of the machine room have effectively improved flow uniformity and reduced TKE, which could lead to improved energy efficiency and reduced noise caused by the fan. Furthermore, the configuration of the improved model is likely to lead to reduced turbulence-induced noise, which is an important consideration for practical applications of the cooling system.

The 2D flow profiles were created for both models at the cross-section of $y = 274$ mm, located before entering the condenser for both models, as shown in Fig. 8c. The black arrows on the 2D flow profile represent velocity vectors at each voxel. It is clear that the improved model has a more uniform flow distribution than the reference model. The flow uniformity index, a dimensionless parameter used to quantify the uniformity of fluid flow distribution across a given area of surface, is defined as follows:

$$\gamma = 1 - \frac{1}{2}\sum_{i=1}^{n}\left|\frac{V_i - V_{avg}}{V_{avg}}\right| \cdot \frac{A_i}{A_{tot}} \tag{5}$$

where V_i represents the local velocity in the i th voxel, V_{avg} is the average velocity, A_i denotes the area of the i th voxel, A_{tot} is the cross-section area, and n indicates the number of voxels in the cross-section. A flow uniformity index closer to 1 indicates a highly uniform flow distribution. The results indicate that the proposed structural modifications enhanced the flow uniformity, γ, from 0.73 in the reference model to 0.86 in the improved model, leading to improved energy efficiency.

4. Conclusions

This study used MRV to measure mean velocity and TKE in a refrigerator machine room to increase entering flow uniformity into the condenser and decrease flow-induced noise. The MRV measurement was validated by comparing with an electromagnetic flowmeter, showing less than 2% error. The study identified shape factors causing flow non-uniformity and high TKE and proposed shape improvements for machine room design. Compared to the reference model, the improved model increased flowrate through the condenser by 17.3% and reduced TKE by over 80% in regions higher than 1.0 J/m^3 which can lead to improved energy efficiency and reduced flow-induced noise. Further research is needed to determine actual noise reduction, but MRV provides useful flow characteristics for CFD verification. It is worth noting that MRV is capable of measuring all three components of velocity vectors in 3D space. Future research can analyze fan noise, and MRV can be applied to models with built-in fans.

Declaration of Competing Interest

The authors declare that they have no known competing financial interests or personal relationships that could have appeared to influence the work reported in this paper.

CRediT authorship contribution statement

Hangfei Dong: Data curation, Writing – original draft, Software, Validation, Visualization, Investigation, Formal analysis. **Chaehyuk Im:** Software, Investigation, Formal analysis. **Chiho Kang:** Conceptualization, Supervision. **Jee-Hyun Cho:** Resources, Methodology, Supervision. **Ilhoon Jang:** Supervision, Writing – review & editing, Project administration. **Simon Song:** Conceptualization, Methodology, Investigation, Supervision, Writing – review & editing, Funding acquisition.

Data availability

Data will be made available on request.

Acknowledgment

This work was supported by the National Research Foundation of Korea (NRF) grant funded by the Korea government (No. 2021R1A2B5B03002103 and No. 2022R1A5A1022977)

Supplementary materials

Supplementary material associated with this article can be found, in the online version, at doi:10.1016/j.ijheatmasstransfer.2023.124446.

References

[1] J.M. Belman-Flores, J.M. Barroso-Maldonado, A.P. Rodríguez-Muñoz, G. Camacho-Vázquez, Enhancements in domestic refrigeration, approaching a sustainable refrigerator – a review, Renew. Sustain. Energy Rev. 51 (2015) 955–968.
[2] S. Lee, S. Heo, C. Cheong, Prediction and reduction of internal blade-passing frequency noise of the centrifugal fan in a refrigerator, Int. J. Refrig. 33 (2010) 1129–1141.
[3] J. Fan, S. Lee, S. Kang, J. Cho, Y. Cho, E. Yeom, Design of drain hole for household refrigerator fan module based on experiments and CFD simulation, Appl. Therm. Eng. 219 (2023) 119567.
[4] J. Hyuk Wie, H. Woo Cho, Y. Gap Park, Y. Soo Kim, Y. Min Seo, M. Yeong Ha, Temperature uniformity analysis of a domestic refrigerator with different multi-duct shapes, Appl. Therm. Eng. 188 (2021) 116604.
[5] Z. He, D. Li, Y. Han, M. Zhou, Z. Xing, X. Wang, Noise control of a twin-screw refrigeration compressor, Int. J. Refrig. 124 (2021) 30–42.
[6] J.B. Freund, Noise sources in a low-Reynolds-number turbulent jet at Mach 0.9, J. Fluid Mech. 438 (2001) 277–305.
[7] R.D. Sandberg, N.D. Sandham, Direct numerical simulation of turbulent flow past a trailing edge and the associated noise generation, J. Fluid Mech. 596 (2008) 353–385.
[8] O. Laguerre, M.H. Hoang, V. Osswald, D. Flick, Experimental study of heat transfer and air flow in a refrigerated display cabinet, J. Food Eng. 113 (2012) 310–321.
[9] S. Marinetti, G. Cavazzini, L. Fedele, F. De Zan, P. Schiesaro, Air velocity distribution analysis in the air duct of a display cabinet by PIV technique, Int. J. Refrig. 35 (2012) 2321–2331.
[10] D.K. Kim, Experimental and numerical study on performance enhancement by modifying the flow channel in the mechanical chamber room of a home refrigerator, Appl. Sci. 10 (2020).
[11] C.J. Elkins, M.T. Alley, Magnetic resonance velocimetry: applications of magnetic resonance imaging in the measurement of fluid motion, Exp. Fluids 43 (2007) 823–858.
[12] W.B. Buchenberg, F. Wassermann, S. Grundmann, B. Jung, R. Simpson, Acquisition of 3D temperature distributions in fluid flow using proton resonance frequency thermometry, Magn. Reson. Med. 76 (2016) 145–155.
[13] M.J. Benson, C.J. Elkins, P.D. Mobley, M.T. Alley, J.K. Eaton, Three-dimensional concentration field measurements in a mixing layer using magnetic resonance imaging, Exp. Fluids 49 (2010) 43–55.
[14] C.J. Elkins, M.T. Alley, L. Saetran, J.K. Eaton, Three-dimensional magnetic resonance velocimetry measurements of turbulence quantities in complex flow, Exp. Fluids 46 (2009) 285–296.
[15] J. Lee, B. Yang, J.H. Cho, S. Song, Velocity and pressure visualization of three--dimensional flow in porous textiles, Text. Res. J. 89 (2019) 5041–5052.
[16] F.T. Davidson, D. Helmer, C. Parker, L. Cox, K. Kahn, C.J. Elkins, J.P. Clark, N. Humbert, B.P. Van Poppel, M.J. Benson, Detailed velocity and heat transfer measurements of an advanced insert for impingement cooling, Int. J. Heat Mass Transf. 185 (2022) 122066.
[17] S. Baek, D. Kook, C. Kim, M. Bang, W. Hwang, Investigation of the relationship between the 3D flow structure and surface heat transfer within a realistic gas turbine blade trailing edge internal serpentine cooling channel, Int. J. Heat Mass Transf. 198 (2022) 123357.
[18] S. Schmidt, K. John, S.J. Kim, S. Flassbeck, S. Schmitter, M. Bruschewski, Reynolds stress tensor measurements using magnetic resonance velocimetry: expansion of the dynamic measurement range and analysis of systematic measurement errors, Exp. Fluids 62 (2021) 121.
[19] S. Ko, B. Yang, J.H. Cho, J. Lee, S. Song, Novel and facile criterion to assess the accuracy of WSS estimation by 4D flow MRI, Med. Image Anal. 53 (2019) 95–103.
[20] N.J. Pelc, M.A. Bernstein, A. Shimakawa, G.H. Glover, Encoding strategies for three-direction phase-contrast MR imaging of flow, J. Magn. Reson. Imaging 1 (1991) 405–413.
[21] J. Lee, A.N. Gupta, L.E. Ma, M.B. Scott, O.R. Mason, E. Wu, J.D. Thomas, M. Markl, Valvular regurgitation flow jet assessment using in vitro 4D flow MRI: implication for mitral regurgitation, Magn. Reson. Med. 87 (2022) 1923–1937.
[22] C.J. Elkins, M. Markl, N. Pelc, J.K. Eaton, 4D Magnetic resonance velocimetry for mean velocity measurements in complex turbulent flows, Exp. Fluids 34 (2003) 494–503.
[23] B. Yang, J.H. Cho, J. Lee, S. Song, Development of custom-made RF coil for magnetic resonance velocimeter with a high spatial resolution, J. Mech. Sci. Technol. 33 (2019) 1681–1688.
[24] J. Lee, S. Ko, J.H. Cho, S. Song, Validation of magnetic resonance velocimetry for mean velocity measurements of turbulent flows in a circular pipe, J. Mech. Sci. Technol. 31 (2017) 1275–1282.
[25] M. Bruschewski, D. Freudenhammer, W.B. Buchenberg, H.P. Schiffer, S. Grundmann, Estimation of the measurement uncertainty in magnetic resonance velocimetry based on statistical models, Exp. Fluids 57 (2016) 83.
[26] P. Dyverfeldt, A. Sigfridsson, J.P. Kvitting, T. Ebbers, Quantification of intravoxel velocity standard deviation and turbulence intensity by generalizing phase–contrast MRI, Magn. Reson. Med. 56 (2006) 850–858.
[27] P. Dyverfeldt, R. Gårdhagen, A. Sigfridsson, M. Karlsson, T. Ebbers, On MRI turbulence quantification, Magn. Reson. Imaging 27 (2009) 913–922.
[28] M.J. Benson, A.J. Banko, C.J. Elkins, D.G. An, S. Song, M. Bruschewski, S. Grundmann, D.D. Borup, J.K. Eaton, The 2019 MRV challenge: turbulent flow through a U-bend, Exp. Fluids 61 (2020) 148.
[29] M.J. Benson, A.J. Banko, C.J. Elkins, D.G. An, S. Song, M. Bruschewski, S. Grundmann, T. Bandopadhyay, L.V. Roca, B. Sutton, K. Han, W. Hwang, J.K. Eaton, MRV challenge 2: phase locked turbulent measurements in a roughness array, Exp. Fluids 64 (2023) 28.